Electronic Structure, Excited States, and Photoelectron Spectra of Uranium, Thorium, and Zirconium Bis(Ketimido) Complexes $(C_5R_5)_2M[-NCPh_2]_2$ (M = Th, U, Zr; R = H, CH_3)

Aurora E. Clark,* Richard L. Martin, and P. Jeffrey Hay

Theoretical Division, Los Alamos National Laboratory, Mail Stop B268, Los Alamos, New Mexico 87545

Jennifer C. Green

Inorganic Chemistry Laboratory, University of Oxford, South Parks Road, Oxford, OX1 3QR, United Kingdom

Kimberly C. Jantunen and Jaqueline L. Kiplinger

Chemistry Division, Los Alamos National Laboratory, Mail Stop J514, Los Alamos, New Mexico 87545

Received: January 19, 2005; In Final Form: April 18, 2005

Organometallic actinide bis(ketimide) complexes $(C_5Me_5)_2An[-N{=}C(Ph)(R)]_2$ (where R = Ph, Me, and CH_2Ph) of thorium(IV) and uranium(IV) have recently been synthesized that exhibit chemical, structural, and spectroscopic (UV−Visible, resonance-enhanced Raman) evidence for unusual actinide−ligand bonding. [Da Re et al., *J. Am. Chem. Soc*., **2005**, *127*, 682; Jantunen et al., *Organometallics*, **2004**, *23*, 4682; Morris et al., *Organometallics*, **2004**, *23*, 5142.] Similar evidence has been observed for the group 4 analogue $(C_5H_5)_2Zr[-N{=}CPh_2]_2$. [Da Re et al., *J. Am. Chem. Soc*., **2005**, *127*, 682.] These compounds have important implications for the development of new heavy-element systems that possess novel electronic and magnetic properties. Here, we have investigated M-ketimido bonding (M = Th, U, Zr), as well as the spectroscopic properties of the highly colored bis-ketimido complexes, using density functional theory (DFT). Photoelectron spectroscopy (PES) has been used to experimentally elucidate the ground-state electronic structure of the thorium and uranium systems. Careful examination of the ground-state electronic structure, as well as a detailed modeling of the photoelectron spectra, reveals similar bonding interactions between the thorium and uranium compounds. Using time-dependent DFT (TDDFT), we have assigned the bands in the previously reported UV−Visible spectra for $(C_5Me_5)_2Th[-N{=}CPh_2]_2$, $(C_5Me_5)_2U[-N{=}CPh_2]_2$, and $(C_5H_5)_2Zr[-N{=}CPh_2]_2$. The low-energy transitions are attributed to ligand-localized N $p \rightarrow$ C=N π^* excitations. These excited states may be either localized on a single ketimido unit or may be of the ligand−ligand charge-transfer type. Higher-energy transitions are cyclopentadienyl $\pi \rightarrow$ CN π^* or cyclopentadienyl $\pi \rightarrow$ phenyl π^* in character. The lowest-energy excitation in the $(C_5Me_5)_2U[-N{=}Ph_2]_2$ compound is attributed to *f*−*f* and metal−ligand charge-transfer transitions that are not available in the thorium and zirconium analogues. Geometry optimization and vibrational analysis of the lowest-energy triplet state of the zirconium and thorium compounds also aids in the assignment and understanding of the resonance-enhanced Raman data that has recently been reported. [Da Re et al., *J. Am. Chem. Soc*., **2005**, *127*, 682.]

Introduction

The chemistry of bent metallocene complexes has been extensively studied with organometallic group 4 elements $(C_5H_5)_2ML_2$ (where M = Ti, Zr, Hf; L = halogen)[1,2] as well as with organoactinide complexes $(C_5Me_5)_2AnL_2$ (where An = Th, U; L = Ph, CH_2Ph, CH_3).[3,4] The bonding and electronic properties have also been investigated with a variety of techniques, such as ultraviolet−visible (UV−Vis) spectroscopy, cyclic voltammetry, and photoelectron spectroscopy (PES).[1−3,5,6] Recently, organoactinide species $(C_5Me_5)_2AnL_2$ of thorium(IV) and uranium(IV) that involve organic ketimido [L = $-N{=}C(R)(R')$] ligands have been synthesized.[3,4] In particular, the ketimido complexes exhibit structural and spectroscopic evidence for an actinide−ligand bond order that may be slightly greater than one. This has important implications for the development of new actinide systems that possess novel electronic and magnetic properties, where the electronic structure of the metal can couple intimately with the ligand.

The electronic properties of group 4 metallocene complexes such as $(C_5H_5)_2MCl_2$ (where M = Ti, Zr, Hf) have been probed using absorption and electronic luminescence spectroscopies.[1,2] These metallocenes are formally d^0 complexes, and their excited states are ligand-to-metal charge-transfer (LMCT) in character. Excitations can arise both from orbitals on the halogen (Cl → M) and the cyclopentadienyl (C_5H_5 → M), and assignments of the photoelectron and absorption spectra show both types of charge-transfer excitations to be close in energy.[1,2] Recent density functional theory (DFT) calculations have provided more insight into the nature of the excitations, in which the character of the highest occupied molecular orbital (HOMO) changed from equal mixtures of Cl and C_5H_5 to being more cyclopentadienyl-localized, as one goes from Ti to Zr to Hf.[2] More recently, the emission from $(C_5H_5)_2Ti(NCS)_2$ was studied and intense phosphorescence from a LMCT triplet excited state was

* To whom correspondence should be addressed: auclark@lanl.gov.

10.1021/jp050339d CCC: $30.25
Published on Web 05/28/2005

observed at 77 K.[7] DFT analysis ascribed this excited state to a π(NCS) → *d*(Ti) excitation.

Experimental investigations using PES have probed the bonding of thorium and uranium metallocene and related complexes, usually coupled with DFT or other theoretical methods. Recent examples of these complexes include $(C_5H_5)_2M(CH_2SiMeCH_2)$ (M = Ti, Zr, Mo, Th),[8] $(C_5H_5)_3AnL$ (An = U, Th; L = CH_3, BH_4),[9] and $An[\eta^8\text{-}C_8H_4(1,4\text{-}Si^iPr_3)_2]_2$ (An = Th, U).[10] Earlier studies of the photoelectron spectra of $(C_5Me_5)_2MX_2$ (M = U, Th, Zr; X = CH_3, Cl) complexes have also utilized DFT to interpret bonding.[11,12]

Following the synthesis of the uranium bis(ketimido) complex $(C_5Me_5)_2U[-N{=}CPh_2]_2$ by Kiplinger et al.,[4] additional structures have been reported for thorium and uranium complexes of the type $(C_5Me_5)_2An[-N{=}CPh(R)]_2$, where R = Ph, Me, and CH_2Ph.[3] The structural details of these complexes will be discussed later in this paper, in comparison to the theoretical studies. Although most thorium(IV) complexes with the $6d^05f^0$ configuration are colorless, the thorium bis(ketimido) complexes are orange, possessing weak absorption in the visible region of 450−550 nm (18 000−22 000 cm^{-1}) and strong absorption bands that extend into the UV region up to 300 nm (33 000 cm^{-1}).[5] The red-colored uranium(IV) bis(ketimido) complexes have similar intense broad absorption bands, with weaker bands extending to even lower energy regions in the visible range of 500−700 nm (14 000−20 000 cm^{-1}).[5]

Previous studies by Morris et al.[13] have examined the spectroscopy and electrochemistry of uranium(IV) and thorium(IV) compounds. There, the $(C_5Me_5)_2AnL_2$ species (where L = Cl, SO_3CF_3, CH_3, CH_2Ph, imido (=N-2,4,6-^{t}Bu$_3$C$_6$H$_2$), hydrazonato (η^2-(*N*,*N*′)-R−N−N=CPh_2 (R = CH_3, CH_2Ph, and Ph), and ketimido (−N=C(Ph)(R); R = CH_3, CH_2Ph)) are categorized as Class I, II, and III, respectively, according to increasing molar absorptivity. Ligands in the Class I complexes include σ-donors such as Me, whereas Class II and Class III species are composed of complexes that contain nitrogen-containing ligands that have the capability to interact in both the σ- and π-fashion with the metal. Thus, the complexes in Classes II and III can have multiple bonding character between the An−N and include the hydrazonato (Class II), ketimido, and imido (Class III) actinide compounds. The resonance Raman spectroscopy of An(IV) ketimido complexes was probed in more detail by Da Re et al.[5] The visible near-infrared (Vis-NIR) absorption region for these complexes was deconvoluted into four absorption bands, denoted as bands I−IV. Band I occurs at higher energy (20−22 000 cm^{-1}), whereas bands II−IV extend to lower energy (12 000−20 000 cm^{-1}). Raman bands showing enhancement in symmetric and asymmetric C=N stretching modes are observed upon excitation in band I. This evidence was used to assign band I as arising from ligand-localized (ketimido) excitation. Additional spectroscopic studies of $(C_5Me_5)_2Th[-N{=}CPh_2]_2$ and $(C_5H_5)_2Zr[-N{=}CPh_2]_2$ were performed, facilitating the assignment of bands II−IV to metal-to-ligand charge-transfer excitations.

Although the spectral (UV−Vis and resonance-enhanced Raman) and electrochemical properties of $5f^2$ uranium(IV) complexes and the analogous f^0d^0 thorium(IV) complexes have been studied,[5,13] there have been no theoretical calculations to elucidate and understand their molecular properties. In this work, theoretical and spectroscopic techniques are used to explore the ground- and excited-state electronic structure of thorium, uranium, and zirconium ketimide complexes. PES is used to probe the ground-state bonding properties of the thorium and uranium ketimide compounds, whereas theoretical calculations present a detailed analysis of the recently reported vibrational and UV−Vis spectra of the thorium, uranium, and zirconium complexes.[5] The theoretical calculations utilize DFT to model the photoelectron spectra and describe the ground-state properties, whereas time-dependent DFT (TDDFT) provides a platform to understand and discuss the excited states.

Computational Methods

The calculations presented for $(C_5H_5)_2Th[-N{=}CPh_2]_2$ (**1**), $(C_5H_5)_2Th[-N{=}CH_2]_2$ (**1a**), $(C_5H_5)_2Zr[-N{=}CPh_2]_2$ (**2**), and $(C_5H_5)_2U[-N{=}CPh_2]_2$ (**3**) used the B3LYP hybrid density functional approach,[14,15] as implemented in the Gaussian03 program.[16] The LANL2 effective core potential[17] (ECP) was used to replace the inner 28 electrons of Zr, whereas the Stuttgart relativistic electron effective core potential[18] (RECP) was used to replace the inner 60 electrons of Th and U. The outer core 4*s*, 4*p* and valence 5*s*, 4*d*, and 5*p* electrons of Zr were treated with the uncontracted LANL2DZ basis,[17] whereas the inner core 5*s*, 5*p*, the outer core 5*d*, 6*s*, 6*p* electrons and valence 5*f*, 6*d*, 7*s*, and 7*p* electrons of U and Th were treated using a [6*s* 6*p* 5*d* 3*f*] contracted Gaussian basis. The 6-31G basis[19] was used to treat the C, N, and H atoms, respectively. The geometries of **1**−**3** were optimized and their vibrational frequencies calculated using analytic second derivatives. The structures were verified to be global minima with no imaginary vibrations. The geometries of the first triplet excited states of **1** and **2** were also optimized and confirmed to be global minima.

The photoelectron spectra of **1** and **3** were modeled to first-order by the method of Gelius,[20] in which the one-electron molecular orbital cross section is approximated by

$$\sigma_{MO} = \sum_{AO} c_{AO,MO}\sigma_{AO}$$

where σ_{AO} is a theoretical atomic orbital cross-section value at an energy appropriate for the incident photon source.[21] The coefficient $c_{AO,MO}$ describes the extent to which each atomic orbital contributes to the molecular orbital. This method qualitatively models the effect of orbital delocalization on the intensities.[22] Lichtenberger and colleagues have demonstrated that this approach reasonably describes the cross sections associated with the low-kinetic-energy electrons obtained from sources such as helium(I) and helium(II).[23] Because the thorium ketimido molecular orbitals (MOs) exhibit significant *f* atomic orbital (AO) character and the Th formally has a $7s^26p^66d^2$ atomic electron configuration, no atomic *f* AO cross section is available for Th. As such, we used the *f* cross-section value of U as an approximation. The predicted MO cross-section values were broadened with Gaussian functions with a width of 0.1 eV. The relative energies of all the MOs were then shifted such that the ionization energy of the HOMO matched the lowest-energy ionization peak in the PES. This amounted to a shift of 2.1 and 0.8 eV in the energies of the thorium and uranium ketimido MOs, respectively. Because unrestricted calculations were used on the uranium(IV) compound, the cross-sectional contribution from the α and β orbitals was averaged for the simulation.

The excited electronic states were determined from TDDFT,[24−28] which was performed at the optimized ground-state geometry, using the same functionals, core potentials, and bases. The natural transition orbitals (NTOs) for a given excited state were determined using the formulation of Martin[29,30] that was used in the development version of Gaussian.

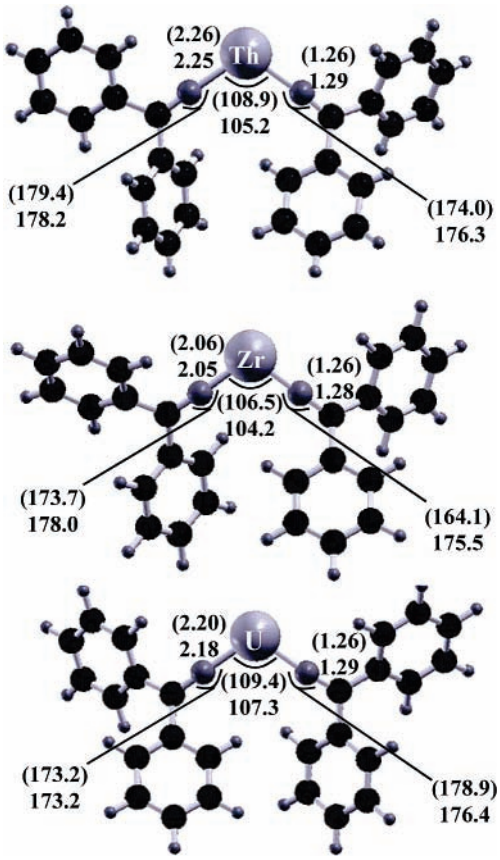

Figure 1. (U)B3LYP optimized geometries of $(C_5H_5)_2Th[-N{=}CPh_2]_2$ (**1**), $(C_5H_5)_2Zr[-N{=}CPh_2]_2$ (**2**), and $(C_5H_5)_2U[-N{=}CPh_2]_2$ (**3**) complexes. Cyclopentadienyl ligands are not shown for clarity. Experimental quantities are given in parentheses, bond lengths are given in angstroms, and bond angles are given in degrees.

Experimental Methods

The compounds $(C_5Me_5)_2Th[-N{=}CPh_2]_2$ (**1***) and $(C_5Me_5)_2U[-N{=}CPh_2]_2$ (**3***) were synthesized as previously reported.[3,4] The helium(I) and helium(II) photoelectron spectra of **1*** and **3*** were obtained using a Helectros model 0078 PE spectrometer that was fitted with a hollow cathode discharge lamp. Spectra were acquired by repeat scanning, using an Atari microprocessor, and calibrated using N_2, Xe, and He, similar to previous reports.[22]

Results and Discussion

1. Ground-State Electronic Structure of $(C_5H_5)_2M[-N{=}CPh_2]_2$ Complexes (M = U, Th, Zr). *1.1. Geometry.* The optimized ground-state structures for $(C_5H_5)_2Th[-N{=}CPh_2]_2$ (**1**), $(C_5H_5)_2Zr[-N{=}CPh_2]_2$ (**2**), and $(C_5H_5)_2U[-N{=}CPh_2]_2$ (**3**) are presented in Figure 1. The structural parameters are quite similar to the X-ray crystal structure values of the permethylated analogues **1*** and **3***, as well as **2** with bond lengths deviating by ±0.03 Å and bond angles deviating by <3°.[3,4,31] Perhaps the largest difference between the gas-phase computed values and the solid-state crystal parameters lies in the relative orientation of the phenyl rings of the ketimido unit, which can deviate by ~10°. Nuclear magnetic resonance (NMR) studies indicate that all of the thorium and uranium complexes are of C_2 symmetry in solution.[3,4] The calculated gas-phase geometries reflect the minor inequivalence of the ketimido ligands found in the solid state.

The crystal structure of the Zr complex,[31] **2**, exhibits a higher degree of nonlinearity along the M−N═C axis, although equivalent M−N and N═C bond lengths are observed. Experimentally, the Zr−N═C bond angle is 164° in one ligand and 174° in the other. The calculated gas-phase structure of **2** is much more similar to the uranium and thorium complexes, with only 5° deviations in the M−N═C bond angle between the bis(ketimido) ligands. Because room-temperature NMR studies of **2** indicate C_2 symmetry similar to **1** and **3**, it is likely that the bending along the Zr−N═C axis in **2** is due to crystal packing effects, rather than differences in Zr−N bonding.

1.2. Bonding. We will now turn to aspects of the bonding in the series of complexes **1**−**3**. The valence molecular orbitals are shown in Figure 2, followed by a detailed analysis of the components of the valence MOs in Table 1. Within the thorium complex (**1**) the HOMO is composed primarily of the lone-pair orbital (N *p*) localized primarily on the N atom of each ketimido ligand (labeled "A" and "B", respectively). Using the N−M−N core to define a plane, this orbital is in-plane antibonding, with respect to the N═C linkage, and minor amplitude is observed on the C_5H_5 rings. The HOMO represents the out-of-phase combination of N *p* AOs, with respect to the bis(−N═CPh_2) linkage (N p_{A-B}). Slightly lower in energy, the HOMO-1 represents the in-phase combination of N *p* AOs across both ligands (N p_{A+B}). Similar contribution of the C_5H_5 rings is observed, relative to the HOMO. As shown in Table 1, there is significant participation of Th 5*f* and 6*d* character in many of the highest five occupied orbitals. The relative contribution is 9% 5*f* (HOMO) and 3% 5*f* and 6% 6*d* (HOMO-1) for the highest occupied pair of orbitals. In the related zirconium complex (**2**), the HOMO and HOMO-1 are similar in character to their thorium counterparts, with similar levels of 4*d* participation.

The total orbital contributions to the Mulliken atomic electron populations in **1** are presented in Table 2. Although the formal charge of Th in **1** is +4.00, the calculated Mulliken charge is +0.98 owing to excess electrons in the 6*p* and 5*f* orbitals. Use of the Natural Population Analysis (NPA) method leads to an estimated Th charge that is ~2.00. This technique uses an occupancy-weighted symmetric transformation to partition AOs into a set of orbitals labeled "core", "valence," and "Rydberg", each of which contribute differently to the density. Here, we follow the recommendations of our previous work,[32] which found that the most consistent NPA results for actinide complexes utilized a valence space that was composed of the 7*s*, 6*d*, and 5*f* orbitals (see Table 1). In this picture, a more-ionic description is observed with a charge of +2.08 on Th that is obtained by the removal of 1.86 electrons from the 7*s* orbital, and the partial transference of a *d* electron to a 5*f* orbital, relative to the $7s^26d^25f^0$ atomic electron configuration. Similar results are obtained by the Mulliken and NPA analysis of the zirconium compound. There, the Mulliken metal charge is +1.11 due to excess electrons in the 4*p* atomic orbital, and the NPA Zr charge is +1.56. In the latter, the valence space was composed of the 5*s* and 4*d* orbitals.

As will be discussed in the next section, the most important orbitals for **1** and **2**, from a spectroscopic standpoint, are the highest two occupied (HOMO and HOMO-1) and lowest two unoccupied orbitals (LUMO and LUMO+1). Figure 2 illustrates that the former are essentially lone-pair orbitals of the N atoms from each ketimido group, whereas the latter are the out-of-plane C═N π^* combinations delocalized across both ketimido linkages, with some π^* character on the phenyl rings. Within **1**, there is an additional 8% 6*d* and 7% 5*f* contribution from the Th center to the LUMO and LUMO+1 orbitals. The higher unoccupied orbitals of **1** have various contributions from Th

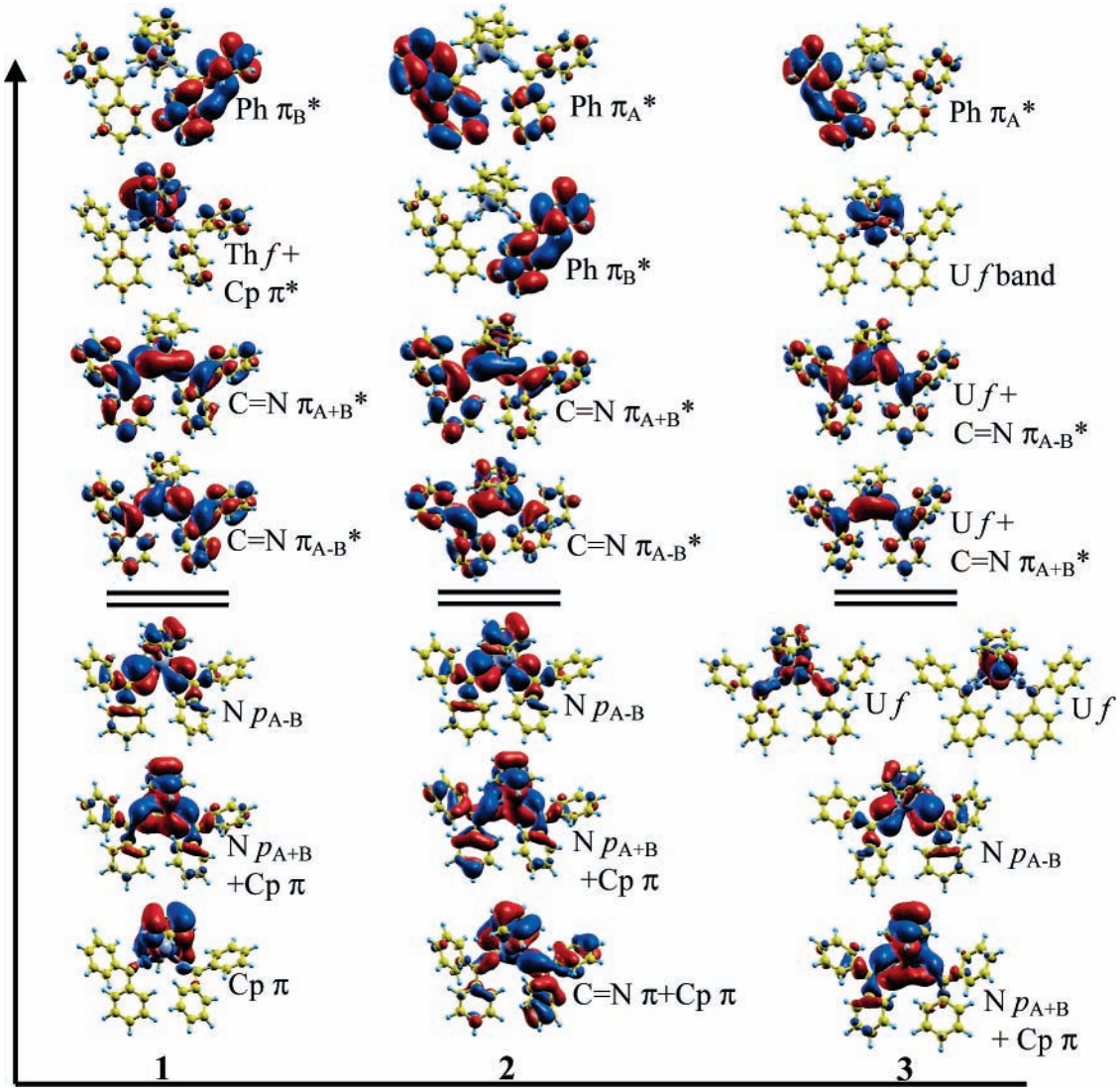

Figure 2. Valence molecular orbitals of $(C_5H_5)_2Th[-N{=}CPh_2]_2$ (**1**), $(C_5H_5)_2Zr[-N{=}CPh_2]_2$ (**2**), and $(C_5H_5)_2U[-N{=}CPh_2]_2$ (**3**), as obtained by density functional theory (DFT). (Cp = C_5H_5, Ph = C_6H_6.)

5*f*, C_5H_5 π* and, at still higher energies, the localized Ph π* orbitals from the ketimido ligands. Again, zirconium, as a second-row transition metal, does not have *f* orbitals, and, consequently, the LUMO+2 through LUMO+5 MOs of **2** are localized Ph π* orbitals. The C_5H_5 π* orbitals lie slightly higher in energy.

The molecular orbital description of the ground electronic structure of the uranium complex (**3**) is similar to that found in **1** and **2**, with the addition of the two unpaired electrons that are essentially 5*f* in nature. With the *xy*−plane being defined by the N−U−N core, the unpaired electrons are primarily $f_{z(x2-y2)}$ and f_{yz2} AOs, as shown in Figure 2, where the two highest α electron orbitals (SOMOs) are plotted. Below these SOMOs are the same pair of ligand-centered orbitals of N *p* character that was observed in **1** and **2**. The Ph π* lie above the unoccupied *f*-orbitals. The orbital contribution to the Mulliken and NPA charges is almost identical to **1**, with the excess electrons clearly present in the 5*f* orbitals.

1.3. Photoelectron Spectroscopy. The helium(I) and helium(II) spectra of the permethylated compounds **1*** and **3*** are given in Figure 3. The behavior of **3***, under experimental conditions, was more tractable than that of **1***, resulting in longer acquisition times and, consequently, higher counts and less background. Four main ionization areas, denoted as A, B, C, and D, are common to both compounds. Ionization energy (IE) values at the band maxima and shoulders are given in Table 3. The IE of corresponding bands has a tendency to be greater for **1*** than **3***. In addition, the uranium compound (**3***) has a low-energy band, *f*, with a maximum at 5.7 eV. This band increases significantly in relative intensity in the helium(II) spectrum and is assigned to ionization of the two *f*-electrons. The high orbital angular momentum of *f* electrons results in delayed maxima in their photoionization cross sections, so the helium(I) band intensity is very low, whereas the helium(II) is relatively high.[33,34] Direct photoionization of the f^2 configuration of uranium(IV) compounds leads predominantly to the $^2F_{5/2}$ ion state of uranium(V), which is the higher-lying $^2F_{7/2}$ state which has too low a cross section.[33] Bands C and D may be assigned to the ligand σ ionizations and the more stable of the π ionizations. Bands A and B are likely to contain ionizations of the upper π orbitals of the phenyl group and the C_5Me_5 rings and ionization from the ketimido ligands.

Photoelectron studies on other C_5Me_5 compounds can give guidance as to where ionizations from the e_1 orbitals of these ligands lie. For example, $(C_5Me_5)_2Fe$ has e_1 bands at 7.31 and 8.08 eV,[6] The divalent lanthanide compounds $(C_5Me_5)_2Ln$ (where Ln = Sm, Eu, and Yb) give C_5Me_5 bands at ~7 eV[35] and $(C_5Me_5)_2UCl_2$ at 7.8 eV.[36] These values suggest that the

TABLE 1: Mulliken Analysis of the Contributions to the Valence Molecular Orbitals in $(C_5H_5)_2Th[-N{=}CPh_2]_2$ (1) and $(C_5H_5)_2Zr[-N{=}CPh_2]_2$ (2), and the α Orbitals of $(C_5H_5)_2U[-N{=}CPh_2]_2$ (3), with Contributions from the Phenyl (Ph) and C=N Units of the A and B Ketimido Ligands, Designated by Subscripts

orbital	*E* (eV)	M *d*	M *f*	C_A	N_A	C_B	N_B	Cp[a]	Ph_A	Ph_B
				1						
LUMO+4	−0.3	2.5	6.4	0.5	0.1	0.0	0.0	10.6	65.4	14.5
LUMO+3	−0.3	2.2	5.4	0.1	0.0	0.5	0.1	10.9	7.1	73.7
LUMO+2	−0.4	16.2	40.6	0.1	0.1	0.2	0.1	29.2	3.2	10.3
LUMO+1	−1.6	7.9	8.0	14.3	10.7	8.0	6.4	3.0	26.9	14.8
LUMO	−1.7	7.4	8.9	8.3	5.4	14.3	10.6	3.3	14.6	27.2
HOMO	−5.3	0.6	9.1	1.1	38.0	0.6	21.7	12.4	10.5	6.0
HOMO-1	−5.5	5.8	3.4	0.8	13.2	1.1	31.8	25.7	6.9	11.3
HOMO-2	−5.9	1.9	1.6	0.3	1.3	0.2	2.9	90.1	0.5	1.2
HOMO-3	−6.0	5.7	4.1	0.1	3.1	1.4	4.3	75.8	1.3	4.2
HOMO-4	−6.2	6.1	1.7	2.1	8.8	0.8	3.5	61.9	12.0	3.1
				2						
LUMO+4	−0.1	4.5		0.2	0.3	0.5	0.3	4.9	23.2	66.1
LUMO+3	−0.1	0.8		0.5	0.1	0.1	0.1	2.5	82.9	13.0
LUMO+2	−0.2	1.7		0.1	0.1	0.5	0.2	3.2	2.9	91.3
LUMO+1	−1.4	16.0		13.5	11.2	6.1	6.5	8.7	27.0	11.0
LUMO	−1.5	13.4		6.0	4.8	13.4	12.1	10.2	10.7	29.4
HOMO	−4.8	0.4		0.8	38.6	0.6	25.4	18.4	9.3	6.5
HOMO-1	−5.6	6.5		3.6	10.5	1.0	20.5	30.3	17.8	9.8
HOMO-2	−6.0	3.9		0.7	2.8	5.4	12.3	44.8	6.6	23.5
HOMO-3	−6.4	10.8		1.5	15.9	0.4	12.7	33.4	17.8	7.5
HOMO-4	−6.6	6.0		0.5	7.1	0.2	0.1	67.5	16.5	1.2
				3						
SOMO+4	−1.2	4.5	81.2	0.8	0.3	0.9	2.7	5.6	1.7	2.3
SOMO+3	−1.5	4.2	84.1	0.1	0.4	0.6	1.0	6.7	0.8	2.1
SOMO+2	−1.7	7.6	32.9	8.4	6.4	7.0	5.1	3.9	15.7	13.0
SOMO+1	−1.9	8.3	37.2	7.6	4.4	9.3	5.1	2.6	12.0	13.5
SOMO	−4.8	3.1	76.6	2.9	0.7	2.7	0.6	7.1	2.9	3.4
SOMO	−5.1	0.5	92.3	0.9	0.3	0.8	0.4	2.1	1.4	1.3
SOMO-1	−5.5	0.7	17.7	0.6	19.0	1.0	32.3	14.4	5.1	9.2
SOMO-2	−5.7	5.5	9.9	0.9	29.4	0.4	7.6	32.0	10.3	4.0
SOMO-3	−5.9	2.3	4.5	0.5	1.1	0.3	1.1	87.8	1.8	0.6
SOMO-4	−6.0	8.6	4.7	0.5	4.4	0.8	9.9	66.7	1.3	3.1

[a] $Cp = C_5H_5$.

TABLE 2: Total Valence Orbital Contribution to the Atomic Populations of $(C_5H_5)_2Th[-N{=}CPh_2]_2$ (1), $(C_5H_5)_2Th[-N{=}CH_2]_2$ (1a), $(C_5H_5)_2Zr[-N{=}CPh_2]_2$ (2), and $(C_5H_5)_2U[-N{=}CPh_2]_2$ (3), as Determined by Mulliken (M) and Natural Population Analyses (NPA)

	1		**1a**		**2**		**3**	
	M[a]	NPA[b]	M	NPA	M	NPA	M	NPA
metal *s*	0.24	0.14	0.25	0.15	0.27	0.16	0.27	0.16
metal *p*	0.24		0.26		0.49		0.11	
metal *d*	1.74	1.26	1.75	1.36	2.13	1.95	1.81	1.32
metal *f*	0.79	0.39	0.75	0.38			2.75	2.78
q metal	0.98	2.08	0.99	2.02	1.11	1.56	1.06	1.70
C *s* in CN_A	2.72	0.83	2.72	1.03	2.71	0.78	2.72	0.83
C *p* in CN_A	3.18	2.84	3.35	3.00	3.23	2.92	3.17	2.85
N *s* in CN_A	2.80	1.48	2.81	1.49	2.80	1.40	2.81	1.45
N *p* in CN_A	4.80	4.39	4.70	4.33	4.78	4.32	4.78	4.29
C *s* in CN_B	2.72	0.83	2.72	1.03	2.71	0.78	2.72	0.83
C *p* in CN_B	3.18	2.84	3.34	3.00	3.23	2.93	3.17	2.85
N *s* in CN_B	2.80	1.48	2.81	1.49	2.80	1.40	2.81	1.45
N *p* in CN_B	4.81	4.40	4.70	4.33	4.77	4.30	4.77	4.28

[a] Valence populations with Mulliken analysis obtained by subtracting the core contribution (up to 6*s*, 6*p*, 5*d*, and 5*f* for Th, and U; up to 4*s*, 4*p* for Zr) on the metal center. [b] NPA analysis used a valence space comprised of the 7*s*, 6*s*, and 5*f* for Th and U, and the 5*s* and 4*d* for Zr, and the 2*s* and 2*p* on C and N.

C_5Me_5 ionizations are more likely to occur in band A than band B, and possibly for **3*,** are the origin of band A2. Phenyl groups have their highest π ionizations in the region of 9 eV[37] and, thus, are likely to contribute to band B.

To seek confirmation of these assignments and to assign the ketimido bands, DFT calculations coupled with experimental atomic photoionization cross sections (see Computational Details) were used to simulate the helium(I) spectra for the model cyclopentadienyl compounds **1** and **3** (Figure 4). Generally, there is good qualitative agreement between the number of bands, as well as the transferability of the ionization intensities, between the two compounds. The nature of the MOs that are ionized in each band is presented in Table 3. Band I, which is compared with band A in the experimental spectrum, beginning at ∼7.3 eV and ending at ∼8 eV, is represented as a shoulder within the simulated spectrum, with a maximum at 7.5 eV. This band has contributions from the N lone-pair orbitals. The maximum of band II at 8.4 eV has contributions from the C_5H_5 π orbitals. The experimental study was performed on $(C_5Me_5)_2Th[-N{=}CPh_2]_2$ (**1***); thus, in the experimental spectrum, we anticipate that the C_5Me_5 feature will be shifted by ∼1 eV to lower bonding energy,[38] placing it with band A, as discussed previously. Meanwhile, band III, which corresponds to band B, beginning at ∼8.7 eV and ending at ∼10.0 eV, can be attributed to the ionization of Ph π orbitals localized on the ketimido ligands (9.1 eV in the simulated spectrum). Band IV, which is incredibly broad in the experimental spectrum, is seen to be composed of two dominant features in the simulated spectrum (11.1 and 12.2 eV) that result from ionization of MOs within the 10.0−13.5 eV energy regime. The lowest-energy feature (band IVa) has a peak at 11.1 eV and is the result of the ionization of the CN π orbitals. In pentamethylcyclopentadienyl compounds, the C_5Me_5 ionizations extend into the 10-eV region.[6] The higher-energy broad feature, band IVb, has contributions from the totally symmetric phenyl π and C_5H_5 π orbitals. In the latter, there is significant C_5H_5-M bonding character. Band V is similarly broad and can be seen to be composed of two features, bands Va and Vb, that are derived from phenyl C−H σ bonding orbitals with calculated IE values of 13.9 and 14.6 eV. Still higher in energy, there are bands originating from C_5H_5 C−H σ (16.6 eV), Ph C−C σ (18.8 eV), and C_5H_5 C−C σ (21.1 eV) orbitals.

The simulated spectrum of **3** is similar to that of **1**, with the exception of a distinct low-energy transition (band Ia) at 5.7 eV that is derived from the ionization of the singly occupied *f* orbitals in the uranium complex (*f*-band). The remaining, higher-energy transitions are predicted to occur at lower IE values but with the same relative intensity for both complexes. A careful comparison of the atomic orbital contributions to the phenyl π MOs that contribute to band III reveals that there is significantly more metal participation in these MOs in **3**, relative to **1**. The enhanced metal character in **3** is attributed to 6p and 6d AOs that contribute to the ketimido π MO in only a minor way (2%−6%); however, that is absent in the thorium compound.

2. Excited Electronic States of $(C_5H_5)_2M[-N{=}CPh_2]_2$ Complexes (M = Th, U, Zr). *2.1. Results of TDDFT Calculations.* The basic orbital structure of the electronic ground state of the ketimido complexes was summarized in the previous section from ground-state DFT calculations. Here, we will use the results of TDDFT calculations to provide a description of the excited states for the thorium (**1**) and zirconium (**2**) species, which have closed-shell singlet ground states. The triplet nature of the uranium compound prohibits us from using TDDFT. Moreover, we use the zirconium compound, as well as a simplified version of the thorium compound **1a**, to assess the nature of high-energy excited states of **1**. TDDFT provides a description of an excited state in terms of all possible single excitations from occupied to virtual orbitals. For a given state,

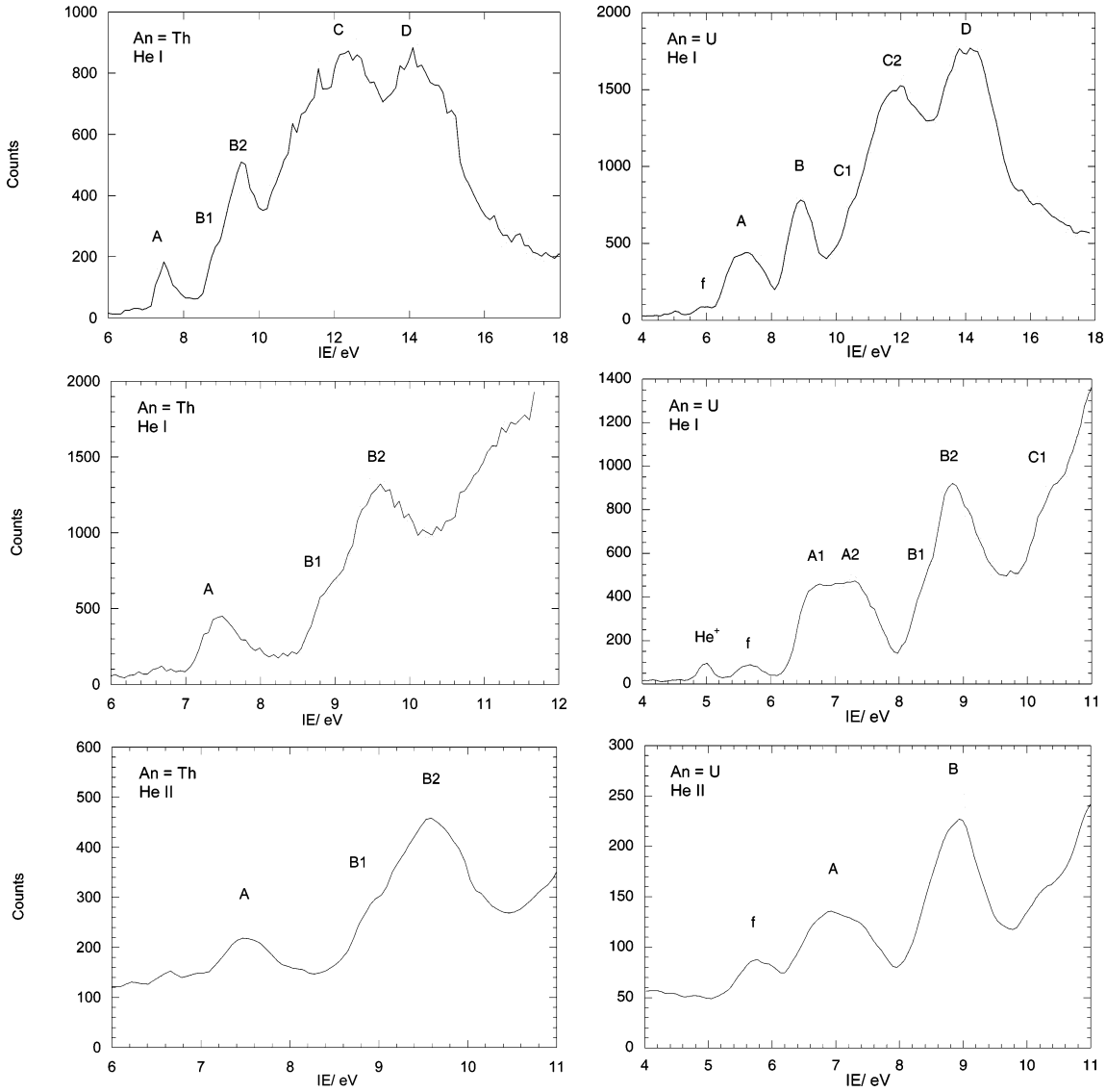

Figure 3. Helium(I) and helium(II) photoelectron spectra of $(C_5Me_5)_2An[-N{=}CPh_2]_2$, for An = Th (**1***) and U (**3***).

TABLE 3: Principal Ionization Features (eV) of $(C_5Me_5)_2Th[-N{=}CPh_2]_2$ (1*) and $(C_5Me_5)_2U[-N{=}CPh_2]_2$ (3*) Observed in Figure 3, as Well as Features in the Simulated Spectra of $(C_5H_5)_2Th[-N{=}CPh_2]_2$ (1) and $(C_5H_5)_2U[-N{=}CPh_2]_2$ (3) Observed in Figure 4[a]

band	f	A	B	C	D
1*		7.47	8.91 9.60	12.40	14.10
3*	5.67	6.72 7.30	8.38 8.84	10.40 11.70	14.00
assignment	*f*	N 2*p* Cp* π e_1	Ph π		

band	Ia	I	II	III	IVa	IVb	Va	Vb
1		7.47	8.36	9.10	11.01	12.17	13.89	14.61
3	5.67	6.34	6.78	7.73	9.57	10.65	12.48	13.20
assignment	*f*	N 2*p*	C_p π e_1	Ph π	CN π	Ph π^b + Cp π^b	Ph C−H σ	Cp C−H σ

[a] Cp* = C_5Me_5; Cp = C_5H_5; Ph = C_6H_6. [b] Totally symmetric π MO.

the most important of these "amplitudes" are given in terms of the pair of orbitals involved in the excitation and the relative percent contribution of each excitation. In typical cases, there are several contributors to a given state in the TDDFT results. One can clarify the interpretation using a natural transition orbital (NTO) analysis, which provides the most compact description of the state by a rotation of the occupied and virtual orbitals that diagonalizes the transition density matrix that connects the ground and excited state. In most cases, the overall description reduces to a single configuration of "hole" and a "particle" NTOs for a given state. The fraction of the total transition density that can be recovered by a particular hole−particle pair is given by its eigenvalue.

We first consider the results for the $(C_5H_5)_2Th[-N{=}CPh_2]_2$ complex (**1**), which corresponds to the actual experimental species except for the replacement of C_5Me_5 by C_5H_5. The results show a set of two almost-degenerate triplet states (T1 and T2) at 2.4 eV (516 nm) and, at slightly higher energy, two

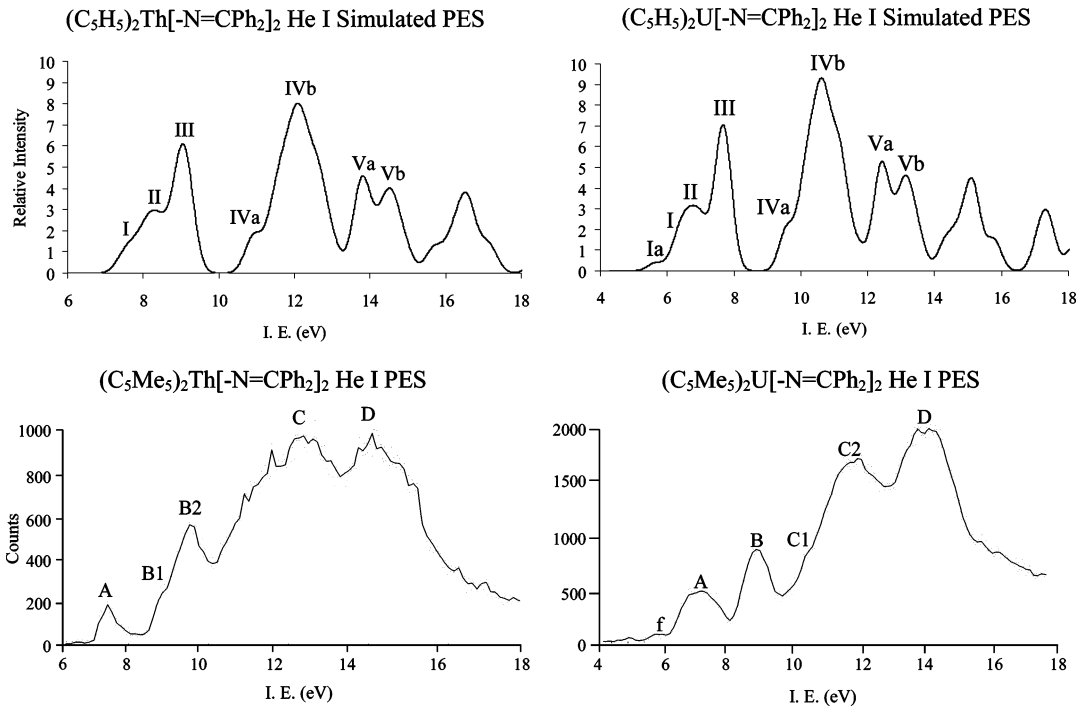

Figure 4. Comparison of the experimental helium(I) photoelectron spectra of $(C_5Me_5)_2Th[-N{=}CPh_2]_2$ (**1***) and $(C_5Me_5)_2U[-N{=}CPh_2]_2$ (**3***) with the simulated spectra of $(C_5H_5)_2Th[-N{=}CPh_2]_2$ (**1**) and $(C_5H_5)_2U[-N{=}CPh_2]_2$ (**3**) obtained by the Gelius model[20] from the DFT molecular orbitals and their energies.

TABLE 4: TDDFT Results for the Optically Allowed Transitions in $(C_5H_5)_2Th[-N{=}CPh_2]_2$ (1), $(C_5H_5)_2Th[-N{=}CH_2]_2$ (1a), and $(C_5H_5)_2Zr[-N{=}CPh_2]_2$ (2)[a]

state	Energy, *E* (eV)	Energy, *E* (nm)	oscillator strength, f	configuration[b]	contribution of the configuration to the noted excited state, %	excitation[c]
				1		
S1	2.7	461.0	0.0077	H → L	50.8	N p_A → CN π_A*
				H → L+1	31.4	
S2	2.8	451.4	0.0049	H-1 → L	34.9	N p_B → CN π_B*
				H-1 → L+1	37.9	
S3	3.3	374.4	0.0037	H-1 → L	48.5	N p_A → CN π_B*
				H → L	23.8	
S4	3.5	357.2	0.0112	H-1 → L+1	75.9	N p_B → CN π_A*
				1a		
S1	2.8	437.0	0.002	H → L	78.0	N p_{A-B} → CN π_{A-B}*
S2	2.9	423.5	0.0003	H → L+1	63.0	N p_{A-B} → CN π_{A+B}*
S3	3.7	335.9	0.0005	H-1 → L	63.2	N p_B → CN π_B*
S4	3.8	327.4	0.0006	H-1 → L+1	75.2	N p_A → CN π_A*
S5	3.9	321.2	0.0003	H → L+2	97.0	N p_{A-B} → Cp π*
S6	4.1	302.6	0.0011	H → L+4	72.8	N p_{A-B} → CN π*
S7	4.1	301.5	0.0100	H-3 → L	72.4	Cp π → CN π_{A+B}*
S8	4.1	300.1	0.0440	H → L+3	83.8	N p_{A-B} π → Cp π*
S9	4.2	295.1	0.0004	H → L+5	94.8	Np_{A-B} → Cp π*
S10	4.2	292.6	0.0170	H-3 → L	88.3	Cp π → CN π_{A-B}*
				2		
S1	2.4	526.8	0.0109	H → L	70.6	N p_{A-B} → CN π_{A-B}*
S2	2.4	514.8	0.0062	H → L+1	70.4	N p_{A-B} → CN π_{A+B}*
S3	3.3	371.7	0.0143	H-1 → L	72.8	N p_{A+B} → CN π_B*
S4	3.6	346.5	0.1491	H-1 → L+1	73.0	N p_{A+B} → CN π_A*
S5	3.9	320.9	0.0126	H-2 → L+1	51.0	Cp π → CN π_A*
				H-3 → L	36.0	
S6	3.9	313.9	0.0596	H → L+2	41.5	Cp π + CN π_{A+B} → CN π_B* + Ph π*
				H-2 → L+1	22.4	
S7	4.0	312.5	0.2469	H → L+2	41.5	Cp π + CN π_{A+B} → CN π_B* + Ph π*
				H-2 → L	21.0	
S8	4.0	309.0	0.0009	H → L+3	64.7	N p_{A-B} → Ph π*
S9	4.0	308.7	0.0328	H → L+4	29.7	N p_{A-B} → Ph π*
				H → L+3	22.5	
S10	4.0	305.0	0.0933	H → L+4	24.6	N p_{A-B} → Ph π*
				H → L+5	21.8	

[a] Cp = C_5H_5; Ph = C_6H_6. [b] The configuration represents the orbitals involved in the transition. [c] Characterization of the excitation based upon the NTOs presented in Figures 5−7.

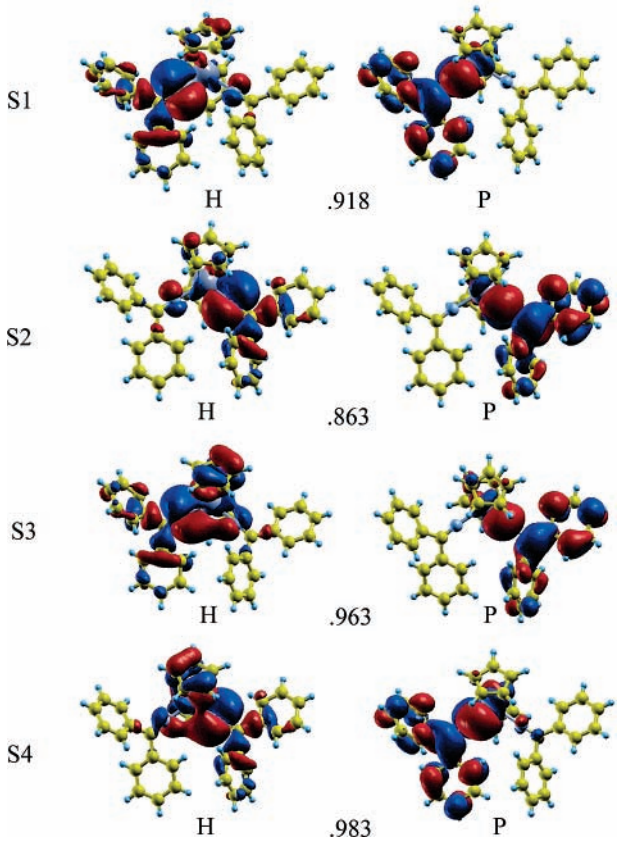

Figure 5. Hole (H) and particle (P) natural transition orbitals (NTOs) for the first four singlet excited states (S1−S4) of $(C_5H_5)_2Th[-N{=}CPh_2]_2$ (**1**), with their respective eigenvalues, as obtained from time-dependent DFT (TDDFT). The eigenvalue is a measure of the fraction of the total transition density that can be recovered by the hole−particle pair.

corresponding singlet states (S1 and S2), at 2.7 eV (451 nm) (Table 4). All four states are comprised of excitations involving the HOMO and HOMO-1 and the LUMO and LUMO+1.

Typically, there are at least two single excitations, in terms of the ground-state orbitals, that are important in the TDDFT description of each state. As we recall from the previous section, the two HOMOs are principally linear combinations of the "in-plane" nitrogen lone pairs on each ketimido ligand (N p_{A-B} and N p_{A+B}), whereas the two lowest virtual MOs are π^* orbitals that involve the CN linkage with significant delocalization on the phenyl groups, as well as some metal admixture. All four states of **1** are thus described as primarily a ligand-based N $p \rightarrow$ CN π^* excitation. As shown more clearly by the NTO analysis (Figure 5), the S1 singlet state of **1** corresponds to a localized N $p \rightarrow$ CN π^* excitation that involves a hole and particle orbital on the same ketimido ligand, and the S2 state corresponds to its partner on the other ligand. As expected for "n $\rightarrow \pi^*$" excitations, there is relatively weak intensity for such transitions with an oscillator strength of <0.01.

The next singlet state (S3) is calculated at 3.30 eV (374 nm) and also involves excitations among the same set of MOs. As shown in Figure 5, the state is actually a charge-transfer excitation from one ketimido ligand to another ("A" $\rightarrow$ "B"). Nearby in energy lies the fourth singlet excited state that corresponds to the charge transfer in the opposite direction, from the "B" to the "A" ketimido ligands. Because of the electronic complexity of **1**, it became necessary to use a model system $(C_5H_5)_2Th[-N{=}CH_2]_2$ (**1a**) to solve for the higher-energy excited state "wave functions". Comparison of structural parameters, as well as the MOs, and population analyses (see

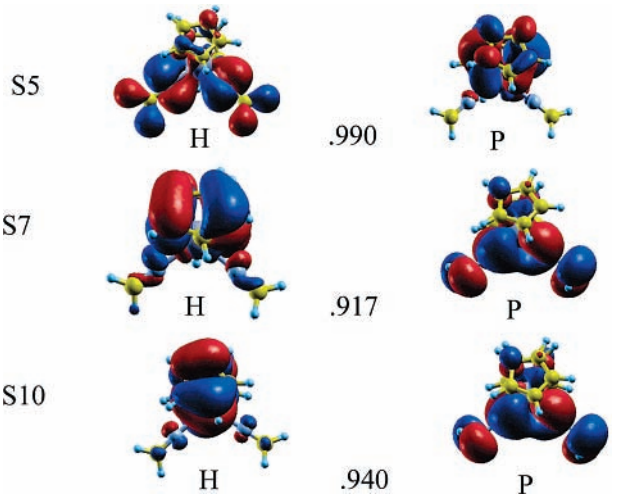

Figure 6. Hole (H) and particle (P) natural transition orbitals (NTOs) for selected high-energy singlet excited states of $(C_5H_5)_2Th[-N{=}CH_2]_2$ (**1a**) with their respective eigenvalues, as obtained from TDDFT.

Table 2) of **1a** indicate that it is quite similar, with regard to the core bonding of the C═N−Th−N═C unit, relative to **1**. Examination of the lowest singlet states of **1a** reveals excitations that are shifted to higher energies by ∼0.4 eV, relative to **1**. However, the overall pattern of the excited states is maintained, with two almost degenerate singlet states, corresponding to excitations within ketimido ligands (S1 and S2) at 2.8 eV, followed by another set (S3 and S4) at 3.7 eV for the interligand N $p \rightarrow$ CN π^* charge-transfer excitations. At higher energies, NTO analysis indicates that the excited states of **1a** are derived from N $p \rightarrow C_5H_5$ π^* excitations, as well as C_5H_5 $\pi \rightarrow$ CN π^* (Figure 6). As expected for C_5H_5 $\pi \rightarrow$ CN π^* excitations, these bands have significant oscillator strength (0.01 and 0.04).

We now examine the excitations in the $(C_5H_5)_2Zr[-N{=}CPh_2]_2$ complex (**2**) (see Table 4) and compare to its thorium(IV) counterpart (**1**). The first four singlet states result from the same set of ligand-based N $p \rightarrow$ CN π^* excitations, as observed in the thorium complex (Figure 5). The first two states are calculated to lie ∼0.3 eV lower in energy in **2**, whereas the third and fourth singlet states are calculated to lie in approximately the same energy region (3.3−3.5 eV, 370−350 nm), relative to **1**. The S5 state, which is similar to the S7 state of **1a (**being C_5H_5 $\pi \rightarrow$ CN π^* in character**)**, lies slightly higher in energy. Higher still are states that result from the excitation of the Ph π^* orbitals from either the C_5H_5 π or CN π orbitals (Figure 7).

2.2. Absorption Spectra and Comparison with Calculations. The experimental electronic absorption spectra of Da Re et. al for $(C_5Me_5)_2Th[-N{=}CPh_2]_2$ (**1***) and $(C_5Me_5)_2U[-N{=}C(Ph)-(CH_2Ph)]_2$ (**4***) are reproduced in Figure 8.[3] Turning first to the features in the spectrum of **1***, a very broad high-energy absorption is observed in the 300−350-nm energy regime. Based on our TDDFT results for **1a** and **2**, we assign this region to either C_5Me_5 $\pi \rightarrow$ Ph* or C_5Me_5 $\pi \rightarrow$ CN π^* transitions. Both of these excitations are symmetry-allowed and account for the high intensity. Lower in energy, and with less oscillator strength, we predict ketimido-localized N $p \rightarrow$ CN π^* transitions. These transitions constitute the localized excitations on each of the "A" and "B" ketimido ligands, as well as the charge-transfer transition from one ketimido ligand to another. This assignment is in sharp contrast to the more delocalized ligand-to-metal charge transfer (LMCT) transitions that have been observed in $(C_5H_5)_2Ti(NCS)_2$ that have been assigned to a π (NCS) $\rightarrow$ *d*(Ti) excitation.[7]

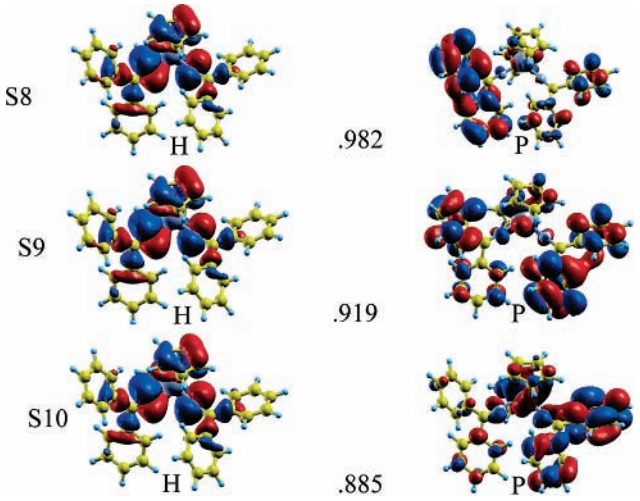

Figure 7. Hole (H) and particle (P) natural transition orbitals (NTOs) for selected high-energy singlet excited states of $(C_5H_5)_2Zr[-N{=}CPh_2]_2$ (**2**) with their respective eigenvalues, as obtained from TDDFT.

Although Figure 8 presents the absorption of $(C_5Me_5)_2U[-N{=}C(Ph)(CH_2Ph)]_2$ (**4***), the very similar spectra of the dark brown-red $(C_5Me_5)_2U[-N{=}CPh_2]_2$ (**3***) complex has recently been obtained by Morris et al. and deconvoluted into four broad bands between 600 nm (15 000 cm^{-1}) and 330 nm (30 000 cm^{-1}) (bands I−IV, Figure 8).[5] Both the phenyl (**3***) and benzyl (**4***) analogues have spectral features that are in sharp contrast to the typical pale-orange-colored compounds that are obtained with simple σ donor ligands.[13] The lower-energy bands are weak and extend through the visible region with more-intense bands observed in the UV region. The energy and intensity of band I is insensitive to metals such as thorium and zirconium, while the lowest-energy bands (bands II−IV) are observed only in the uranium spectra. Given the similarity between the N *p* lone pair and CN π^* MOs in the valence band of the uranium compound (**3***), we assign band I to the N $p \rightarrow$ CN π^* transitions of both the ligand-localized and the ligand−ligand charge-transfer type. Because it is inappropriate to perform TDDFT calculations on a triplet uranium complex, we speculate that the low-energy bands observed at ∼600 nm are metal-to-ligand charge transfer in character and that the lowest-energy transitions are *f*−*f*. This is reasonable, given the singly occupied *f* orbitals of the uranium (**3***) compound and the low-energy CN π^* orbitals that are accessed in the higher-energy excitations. The absence of unpaired 5*f* electrons in the Th and Zr species precludes such features in their spectra.

In contrast to our theoretical findings, previous spectroscopic studies of $(C_5H_5)_2Ti(NCS)_2$,[7] as well as colored thorium(IV) compounds,[39] attributed their low-energy absorptions to visible LMCT transitions. Subsequent examination of the thorium(IV) and uranium(IV) bis(ketimide) compounds concluded that their unique color may be attributed to ligand-localized $\pi \rightarrow \pi^*$ and or metal charge-transfer transitions.[3] Further spectroscopic evidence, including resonance Raman, elucidated that excitation into band I in Figure 8 generated a broken-symmetry excited state.[5]

3. Resonance Raman and Geometries of Triplet Excited States. We now turn to a discussion of the resonance-enhanced Raman vibrational data that has recently been reported by Da Re et al.[5] This technique determines the spectrum of vibrational transitions using the differences in energy between incident and Raman scattered radiation. Resonance is obtained by transition into excited states such as those discussed previously. Coming into resonance with an electronic transition enhances ground-state vibrations within the spectra whose atomic displacements coincide with the optimized geometry of the excited state (Franck−Condon effect). Based on our assignment of the absorption spectra of **1*** and **3***, one would expect enhancement of vibrations associated with the C═N linkage in the ketimido ligand when band I is probed and enhancement of vibrations

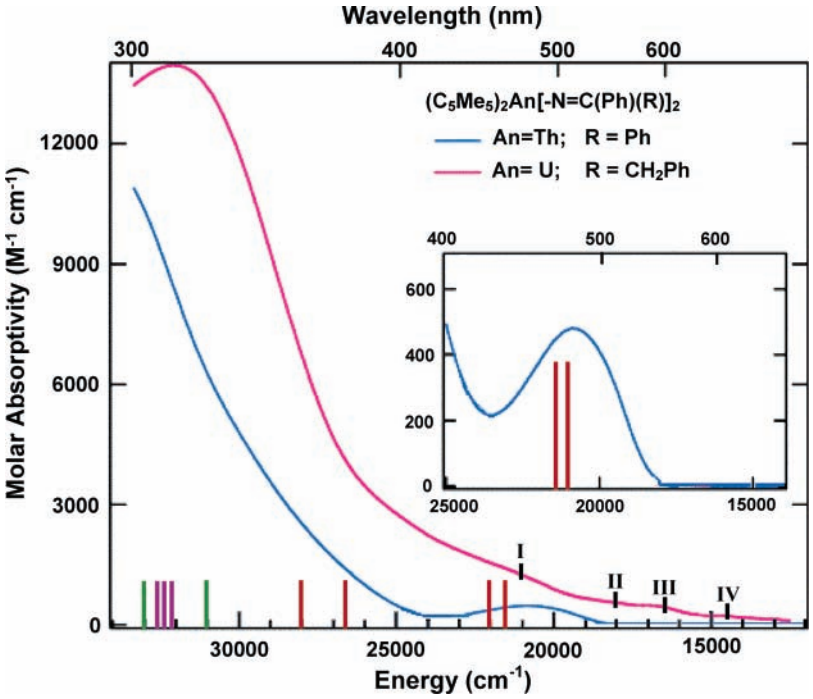

Figure 8. Electronic absorption spectra of ∼1 × 10^{-4} M toluene solutions of $(C_5Me_5)_2Th[-N{=}CPh_2]_2$ (**1***, blue) and $(C_5Me_5)_2U[-N{=}C(Ph)(CH_2Ph)]_2$ (**4***, pink).[2] The four bands that result from the deconvolution of the spectrum of $(C_5Me_5)_2U[-N{=}CPh_2]_2$ (**3***) are labeled I−IV.[5] The predicted low-energy TDDFT transitions of $(C_5H_5)_2Th[-N{=}CPh_2]_2$ (**1**, red), as well as the higher-energy states of $(C_5H_5)_2Th[-N{=}CH_2]_2$ (**1a**, green) and $(C_5H_5)_2Zr[-N{=}CPh_2]_2$ (**2**, purple) are presented as a stick diagram. The 25 000−15 000 cm^{-1} energy regime is magnified in the inset. (Experimental data reproduced with permission of the authors of ref 3. Copyright *Organometallics*, 2004.).

TABLE 5: Calculated Vibrational Data with Assignments for $(C_5H_5)_2Th[-N{=}CPh_2]_2$ (1), $(C_5H_5)_2Zr[-N{=}CPh_2]_2$ (2), and $(C_5H_5)_2U[-N{=}CPh_2]_2$ (3), as Well as the Previously Reported[a] Resonance Raman Data for 2 and $(C_5Me_5)_2U[-N{=}CPh_2]_2$ (3*)[b]

calculated **1**	calculated ^{3}**1**	assignment[c]
1665 (ν_{171})	1660	Ph
1660 (ν_{170})	1654	Ph
1654 (ν_{169})	1642	Ph
1643 (ν_{167})	1631	Ph
1623 (ν_{163})	1603	C=N
1610 (ν_{162})	1547	C=N
1233 (ν_{131})	1234	Ph
1065 (ν_{111})	1060	Ph

resonance Raman **2**	calculated **2**	calculated ^{3}**2**	assignment[c]
1652**	1694 (ν_{171})	1675	C=N
1631**	1674 (ν_{170})	1654	C=N
1593**	1651 (ν_{167})	1632	Ph
1588	1648 (ν_{166})	1648	Ph
1576	1632 (ν_{165})	1631	Ph
1569	1631 (ν_{162})	1629	Ph
1143	1189 (ν_{124})	1187	P
1124	1150 (ν_{123})	1147	Cp

resonance Raman **3***	calculated **3**	assignment[c]
1615**	1607 (ν_{163})	C=N
1607**	1595 (ν_{162})	C=N
1596	1548 (ν_{161})	Ph
1587**	1545 (ν_{159})	Ph
1570	1502 (ν_{157})	Ph
1565	1500 (ν_{154})	Ph
1486	1483 (ν_{150})	Cp
1423	1402 (ν_{149})	Cp
1146	1128 (ν_{121})	Ph
1001	976 (ν_{93})	Ph

[a] From ref 5. [b] Each vibration is given by its frequency (in cm^{-1}) and mode number (ν_{xxx}). Enhanced vibrations in the experimental systems at an excitation wavelength of 514 or 458 nm are labeled with two asterisks (**). Predicted values for the optimized triplet states ^{3}**1** and ^{3}**2** are also presented. [c] Cp = C_5H_5; Ph = C_6H_6.

associated with C_5H_5 and Ph moieties when a higher-energy regime is examined. Indeed, the reported Raman spectra of **2** and **3*** exhibit enhancement of these vibrations, with intensities that vary with excitation wavelength as one comes into resonance with the excited states that contribute to band I.

Here, we have calculated the values of infrared and Raman active vibrations to aid in the assignment of the resonance Raman spectra and to explain the unique vibrational enhancements that have been observed.[5] (See Table 5.) For compound **2**, we predict the symmetric and asymmetric C=N stretches to occur at 1694 and 1674 cm^{-1}, respectively. These compare to experimental values of 1652 and 1631 cm^{-1}.[5] Lower-energy Ph stretches are found in the 1600 cm^{-1} envelope. Generally, the computed vibrational frequencies are shifted to higher energy by 30−40 cm^{-1}, relative to that observed in the experimental system.[5] Slightly better agreement is observed between the vibrational data of $(C_5H_5)_2U[-N{=}CPh_2]_2$ (**3**) and its pentamethylcyclopentadienyl derivative (**3***). There, the symmetric and asymmetric C=N stretches are calculated to occur at 1607 and 1595 cm^{-1}, whereas they are experimentally observed at 1615 and 1607 cm^{-1}, respectively.[5] The relative shift in C=N vibrational frequency to lower energy as one goes from Zr to U is reproduced computationally.

Resonance enhancement has been observed upon excitation into band I (N $p \rightarrow$ CN π^*) for both the symmetric and asymmetric C=N stretching vibrations.[5] Because the symmetry requirements for a Raman transition usually allow only the totally symmetric vibration, the observation of enhancement of the asymmetric C=N stretch indicates that the excited state breaks symmetry. This observation is in excellent agreement with our description of the broken-symmetry N $p \rightarrow$ CN π^* transition that is localized on a given ketimido ligand, rather than a transition that is delocalized in a symmetric fashion across both ligands. Such an assignment is further corroborated by our investigation of the optimized geometry and calculated vibrational properties of the lowest energy triplet states of **1** and **2** (Figure 9).

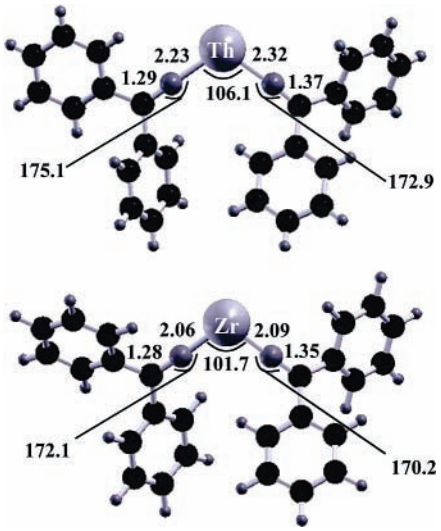

Figure 9. (U)B3LYP optimized geometries of the lowest-energy triplet state of $(C_5H_5)_2Th[-N{=}CPh_2]_2$ (**1**) and $(C_5H_5)_2Zr[-N{=}CPh_2]_2$ (**2**). Cyclopentadienyl ligands are not shown for the purpose of clarity. Bond lengths are given in angstroms, and bond angles are given in degrees.

Because our TDDFT results indicate that the lowest-energy triplet and singlet states are of the same character, differing only in spin, optimization of the first triplet state should be a good approximation to the excited-state geometry probed by excitation into band I. As shown in Figure 9, the largest difference between the ground- and excited-state geometries lies in the C=N bond length of one ketimido ligand. Within the $(C_5H_5)_2Th[-N{=}CPh_2]_2$ (**1**) complex, the C=N bond length increases from 1.29 Å to 1.37 Å, and in the zirconium compound, this distance goes from 1.28 Å to 1.35 Å. Commensurate with the change in bond length is a decrease in the N−C−M angle, from 176.3° to 172.9° in **1** and from 175.5° to 170.2° in **2**. Both of these geometrical differences indicate that the lowest-energy triplet state of both **1** and **2** involves the population of a C=N π^* orbital and that the nominal bond order between the C=N decreases from ∼2 in the ground state to ∼1.5. The computed vibrational data for these triplet states correctly shows an ∼40 cm^{-1} shift in energy of one of the C=N stretches.

Conclusion

The ground-state electronic structure and excited-state properties of the $(C_5Me_5)M[-N{=}CPh_2]_2$ and $(C_5H_5)M[-N{=}CPh_2]_2$ (M = Th, U, Zr) compounds have been examined using photoelectron spectroscopy, as well as density functional theory (DFT) and time-dependent DFT (TDDFT). The unique color of the thorium, uranium, and zirconium compounds is attributed to ligand-localized excitation of the n $\rightarrow \pi^*$ type. These excited states may be either localized on a single ketimido unit or may be of the ligand−ligand charge-transfer type. Higher-energy transitions are C_5H_5 $\pi \rightarrow$ CN π^* or C_5H_5 $\pi \rightarrow$ C_6H_6 π^* in

character. The lowest-energy excitation in the $(C_5Me_5)U[-N=CPh_2]_2$ (**3***) compound is attributed to $f-f$ and metal−ligand charge-transfer transitions that are not available in the thorium and zirconium analogues. Geometry optimization and vibrational analysis of the lowest-energy triplet state of the zirconium and thorium compounds confirms the broken-symmetry ligand-localized character of the lowest-energy singlet excited state. These geometries also help to assign the resonance Raman spectra that has recently been obtained.

Acknowledgment. A.E.C. was supported by a Directors' funded postdoctoral fellowship at Los Alamos National Laboratory. K.C.J. acknowledges fellowship support from the G. T. Seaborg Institute for Transactinium Science at Los Alamos. Support for this research was provided by the United States Department of Energy, Office of Science, Office of Basic Energy Science under the auspices of the Heavy Element Chemistry Program and the Los Alamos National Laboratory's Laboratory Directed Research and Development Office.

References and Notes

(1) Kenney, J. W.; Boone, D. R., III; Striplin, D. R.; Chen, Y.-H.; Hamar, K. B. *Organometallics* **1993**, *12*, 3671.

(2) Wang, X.; Chen, L.; Endou, A.; Kubo, M.; Miyamoto, A. *J. Organomet. Chem.* **2003**, *678*, 156.

(3) Jantunen, K. C.; Burns, C. J.; Castro-Rodriguez, I.; Da Re, R. E.; Golden, J. T.; Morris, D. E.; Scott, B. L.; Taw, F. L.; Kiplinger, J. L. *Organometallics* **2004**, *23*, 4682.

(4) Kiplinger, J. L.; Morris, D. E.; Scott, B. L.; Burns, C. J. *Organometallics* **2002**, *21*, 3073.

(5) Da Re, R. E.; Jantunen, K. C.; Golden, J. T.; Kiplinger, J. L.; Morris, D. E. *J. Am. Chem. Soc.* **2005**, *127*, 682.

(6) Cauletti, C.; Clark, J. P.; Green, J. C.; Jackson, S. E.; Fragala, I. L.; Ciliberto, E.; Coleman, A. W. *J. Electron. Spectrosc. Relat. Phenom.* **1980**, *18*, 61.

(7) Patrick, E. L.; Ray, C. J.; Meyer, G. D.; Ortiz, T. P.; Marshall, J. A.; Brozik, J. A.; Summers, M. A.; Kenney, J. W., III. *J. Am. Chem. Soc.* **2003**, *125*, 5461.

(8) Ciliberto, E.; Di Bella, S.; Gulino, A.; Fragala, I.; Petersen, J. L.; Marks, T. J. *Organometallics* **1992**, *11*, 1727.

(9) Di Bella, S.; Gulino, A.; Lanza, G.; Fragala, I.; Marks, T. J. *J. Phys. Chem.* **1993**, *97*, 11673.

(10) Cloke, F. G. N.; Green, J. C.; Jardine, C. N. *Organometallics* **1999**, *18*, 1080.

(11) Bursten, B. E.; Fang, A. *J. Am. Chem. Soc.* **1983**, *105*, 6495.

(12) Ciliberto, E.; Condorelli, G.; Fagan, P. J.; Manriquez, J. M.; Fragala, I.; Marks, T. J. *J. Am. Chem. Soc.* **1981**, *103*, 4755.

(13) Morris, D. E.; Da Re, R. E.; Jantunen, K. C.; Castro-Trodriguez, I.; Kiplinger, J. L. *Organometallics* **2004**, *23*, 5142.

(14) Lee, C.; Yang, E.; Parr, R. G. *Phys. Rev. B* **1988**, *37*, 785.

(15) Becke, A. D. *Phys. Rev. A* **1988**, *38*, 3098.

(16) Frisch, M. J.; Schlegel, G. W. T., H. B.; Scuseria, G. E.; Robb, M. A.; Cheeseman, J. R.; Montgomery, J. A., Jr.; Vreven, T.; Kudin, K. N.; Burant, J. C.; Millam, J. M.; Iyengar, S. S.; Tomasi, J.; Barone, V.; Mennucci, B.; Cossi, M.; Scalmani, G.; Rega, N.; Petersson, G. A.; Nakatsuji, H.; Hada, M.; Ehara, M.; Toyota, K.; Fukuda, R.; Hasegawa, J.; Ishida, M.; Nakajima, T.; Honda, Y.; Kitao, O.; Nakai, H.; Klene, M.; Li, X.; Knox, J. E.; Hratchian, H. P.; Cross, J. B.; Adamo, C.; Jaramillo, J.; Gomperts, R.; Stratmann, R. E.; Yazyev, O.; Austin, A. J.; Cammi, R.; Pomelli, C.; Ochterski, J. W.; Ayala, P. Y.; Morokuma, K.; Voth, G. A.; Salvador, P.; Dannenberg, J. J.; Zakrzewski, V. G.; Dapprich, S.; Daniels, A. D.; Strain, M. C.; Farkas, O.; Malick, D. K.; Rabuck, A. D.; Raghavachari, K.; Foresman, J. B.; Ortiz, J. V.; Cui, Q.; Baboul, A. G.; Clifford, S.; Cioslowski, J.; Stefanov, B. B.; Liu, G.; Liashenko, A.; Piskorz, P.; Komaromi, I.; Martin, R. L.; Fox, D. J.; Keith, T.; Al-Laham, M. A.; Peng, C. Y.; Nanayakkara, A.; Challacombe, M.; Gill, P. M. W.; Johnson, B.; Chen, W.; Wong, M. W.; Gonzalez, C.; Pople, J. A. Gaussian; Revision B.04; Gaussian, Inc.: Pittsburgh, PA, 2003.

(17) Hay, P. J.; Wadt, W. R. *J. Chem. Phys.* **1985**, *82*, 299.

(18) Küchle, W.; Dolg, M.; Stoll, H.; Preuss, H. *J. Chem. Phys.* **1994**, *100*, 7535.

(19) Hehre, W. J.; Ditchfield, R.; Pople, J. A. *J. Chem. Phys.* **1972**, *56*, 2257.

(20) Bancroft, G. M.; Malmquist, P. A.; Svensson, S.; Basilier, E.; Gelius, U.; Seigbahn, K. *Inorg. Chem.* **1978**, *17*, 1595.

(21) Yeh, J. J.; Lindau, I. *Atomic Data and Nuclear Data Tables* **1985**, *32*, 1.

(22) Green, J. C. *Acc. Chem. Res.* **1994**, *27*, 131.

(23) Padden Metzker, J. K.; Gruhn, N. E.; Lichtenberger, D. L. *J. Phys. Chem. A* **2002**, *106*, 9999.

(24) Stratmann, R. E.; Scuseria, G. E.; Frisch, M. J. *J. Chem. Phys.* **1998**, *109*, 8218.

(25) Petersilka, M.; Grossmann, U. J.; Gross, E. K. U. *Phys. Rev. Lett.* **1996**, *76*, 1212.

(26) Bauernschmitt, R.; Alrichs, R.; Hennrich, F. H.; Kappes, M. M. *J. Am. Chem. Soc.* **1998**, *120*, 5052.

(27) Casida, M. E. *J. Chem. Phys.* **1998**, *108*, 4439.

(28) Jamorski, C.; Casida, M. E.; Salahub, D. R. *J. Chem. Phys.* **1996**, *104*, 5134.

(29) Batista, E. R.; Martin, R. L. *Encyclopedia of Computational Chemistry*; Wiley: Chichester, U.K., 2003.

(30) Martin, R. L. *J. Chem. Phys.* **2003**, *118*, 4775.

(31) Erker, G.; Fromberg, W.; Krueger, C.; Raabe, E. *J. Am. Chem. Soc.* **1988**, *110*, 2400.

(32) Clark, A. E.; Sonnenberg, J.; Hay, P. J.; Martin, R. L. *J. Chem. Phys.* **2004**, *121*, 2563.

(33) Downs, A. J.; Egdell, R. G.; Orchard, A. F.; Thomas, P. D. P. *J. Chem. Soc., Dalton Trans.* **1978**, 1755.

(34) Brennan, J. G.; Green, J. C.; Redfern, C. M. *J. Am. Chem. Soc.* **1989**, *111*, 2373.

(35) Andersen, R. A.; Boncella, J.; Green, J. C.; Burns, C. J.; Hohl, D.; Roesch, N. *J. Chem. Soc. Chem. Commun.* **1986**, 405.

(36) Green, J. C.; Kelly, M. R.; Long, J. A.; Kanellakopulos, B.; Yarrow, P. I. W. *J. Organomet. Chem.* **1981**, *212*, 329.

(37) Kimura, K.; Katsumata, S.; Achiba, Y.; Yamazaki, T.; Iwata, S. *Handbook of HeI Photoelectron Spectra of Fundamental Organic Molecules*; Japan Scientific Societies Press: Tokyo, 1981.

(38) Green, J. C. *Struct. Bonding (Berlin, Ger.)* **1981**, *43*, 37.

(39) Cloke, F. G. N.; Hitchcock, P. B. *J. Am. Chem. Soc.* **1997**, *119*, 7899.